Barrier Sensor Based on Plastic Optical Fiber to Determine the Wind Speed at a Wind Generator

Joseba Zubia, O. Aresti, Jon Arrúe, and M. López-Amo

***Abstract*—We have made use of the properties of plastic optical fibers (POFs) to develop a sensor for determining the wind speed in a wind generator. As POFs are easy to handle, flexible, economical, and immune to electromagnetic interference, we have utilized them to design an inexpensive sensor that is not affected by storms, which are one of the major problems in wind generators. Both theoretical and experimental results are presented. Specifically, we study the dynamic characteristics of the sensor by taking into account the light reflections on a mobile surface and by using two different theoretical approaches. The corresponding experimental results corroborate the validity of such approaches.**

***Index Terms*—Plastic optical fiber, POF, fiber sensor, wind speed optical sensor.**

I. Introduction

THE FIELD of fiber optical sensors has developed rapidly over the last years. Specifically, a wide variety of sensors have been described to be able to measure parameters such as concentration of solutions, temperature, pressure, flow and rotation [1]–[4]. Nowadays, plastic optical fibers (POFs) have evolved into a suitable medium for the implementation of sensors, due to the good technical and economical characteristics of such fibers [5]–[7].

In this paper, we report on the design of a POF-based barrier sensor for determining the wind speed in a wind generator. Several designs have been used for this purpose, which in most cases are based on the response of an optocoupler to the light signal obtained by intercepting an emitted light beam by means of several tabs attached to the structure of the anemometer. However, the fact that the optocoupler works with electric signals makes approaches of this type very sensitive to electric sparks. This is an important disadvantage because wind generators are generally installed at the tops of mountains, where sparks are frequent. Specifically, their situation increases the probability of sparks generating induced currents at the top of the wind generator, where the optocoupler is mounted. Although these currents are weak, they frequently damage both the optocoupler and the automaton connected to it. Therefore, such designs lack the necessary electric isolation.

Manuscript received May 4, 2000; revised August 7, 2000. This work was supported by the Departamento de Educación, Universidades e Investigación del Gobierno Vasco Project UE-1998-4, and also by the "Universidad del País Vasco" Project UPV 147.345-EA 152/98 ZUBIA.

J. Zubia and J. Arrúe are with the Departamento de Electrónica y Telecomunicaciones, University of the Basque Country, ESTII, Bilbao, Spain (e-mail: jtpzuzaj@bi.ehu.es).

O. Aresti is with Lambda Comunicaciones Ópticas, Zamudio, Spain.

M. López-Amo is with the Departamento de Ingeniería Eléctrica y Electrónica, Universidad Pública de Navarra, Navarra, Spain.

Publisher Item Identifier S 1077-260X(00)11295-X.

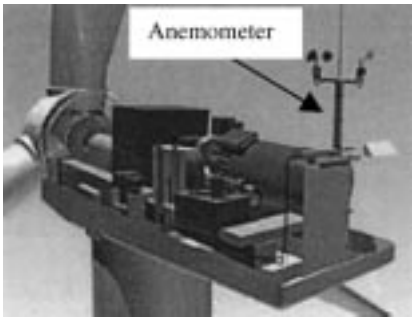

Fig. 1. Wind turbine.

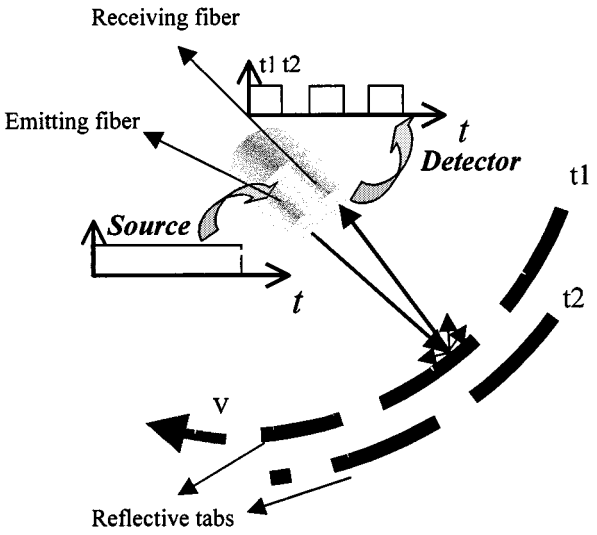

Fig. 2. Structure of the wind speed sensor. It consists of a pair of plastic optical fibers, one emitting light at 660 nm and the other one collecting the light reflected back by the reflective tabs of the hollow slotted cylinder attached to the rotor's vanes of the anemometer. When the wind blows at a speed v, the rotor's vanes move at the same speed as the reflective tabs of the slotted cylinder. Only if the light from the emitting fiber is intercepted by a tab will the light be reflected back.

To overcome this problem, we propose a new fiber optical sensor that gives great electric isolation to the automaton, while yielding an even better performance than conventional encoder equipment. The proposed structure consists of a light emitting POF, a receiving one and a hollow slotted cylinder attached to the vanes of the anemometer's rotor, whose partially reflective tabs periodically intercept the cone of light emitted by the POF (Figs. 1 and 2). In this way, the reflected power can be partially collected by another POF, obtaining a train of light pulses that occur every time a tab completes a full rotation. Specifically, we analyze the influence of the sensor's physical dimensions and the POF's characteristics on the performance of the sensor. We

also study the sensor's response time by analyzing the transient variations in the received optical power.

With this design, we can measure wind speeds from 10 km/h to 100 km/h. The chosen fibers were two 0.49 mm-diameter PMMA POFs. This choice was due to economical and practical reasons. On the one hand, POFs are cheaper and easier to handle than glass fibers, so they are well suited to this kind of application. On the other hand, their large core diameter allows greater manufacture tolerances without worsening the sensor's performance.

The analysis of the wind sensor begins with a description of its structure. Next, we explain the two methods employed for the theoretical analysis, as well as the corresponding results. Then we study the dynamic characteristics of the sensor by taking into account that the reflections occur on a mobile surface. Finally, we present the experimental results obtained.

II. Structure of the Sensor

The sensor employs two step-index PMMA POFs whose core and cladding refractive indices are $n_{\rm co} = 1.492$ and $n_{\rm cl} = 1.417$, respectively. These fibers lie inside the mobile slotted cylinder and they point in the radial direction, as shown in Fig. 2. In the same figure, we have also represented two possible positions of the cylinder's tabs at instants $t1$ and $t2$, for which the reflected power changes from a maximum to zero.

For the emission and reception of light, we used a CONTRINEX LFK-3031-303 fiber optic emitter-receiver in order not to have to mount two separate fibers. This type of emitter-receiver is suitable for our sensor application since it can work in hard weather conditions. The emitter was a visible red LED ($\lambda = 660$ nm). The wind speed v can be related to the number of received pulses per unit of time by means of the expression $v \approx (2\pi RN/n)$, where R is the cylinder's radius (1.2 cm), N is the number of received pulses per unit time, and n is the number of the cylinder's tabs ($n = 6$).

III. Model of the Sensor

The light emitted from one of the fibers is partly coupled into the other one when it reflects on the cylinder's tabs, as depicted in Fig. 3. To analyze this situation we assumed both fibers to have a core of radius "a" and the reflecting surface to be planar. The performance of the sensor is characterized by its "coupling efficiency" $\eta = \mathbf{P}_{\rm received}/\mathbf{P}_{\rm emitted}$, where the numerator and denominator are the received and emitted powers, respectively. This parameter depends on the distance between the fibers and the reflecting surface. Thus, there is an optimum position of the fibers for a maximum coupling efficiency. Fig. 3 also shows the parameters chosen for the analysis of the sensor.

A. Ray Tracing Method

To calculate the coupling efficiency, we can use the ray-tracing method by considering geometric light rays emitted from a series of foci uniformly distributed at the output end of the emission fiber [8]–[10]. Each ray has an associated power that depends on the position of the emission point and on the angular direction of the emitted ray. If we sum the powers of all those rays that are coupled into the reception fiber, as well as the initial powers of all the rays, then we can calculate the coupling efficiency. An upper limit to the number of rays for the analysis to have physical meaning is the number of modes that can propagate along a step index POF. This value is determined by the waveguide parameter $V = (2\pi a/\lambda)(n_{\rm co}^2 - n_{\rm cl}^2)^{1/2}$, where λ is the wavelength of the emitted light. Specifically, the number of modes that can propagate in a highly multimode step-index fiber, such as a POF, is given by $N = V^2/2$ [10]. Since in our case, $\lambda = 660$ nm and $a = 0.49$ mm, we need to consider no more than 2 000 000 rays from a purely theoretical point of view. However, we have already shown that the results obtained with the ray tracing method converge rapidly, so it is enough to consider only 100 000 rays [6], [7].

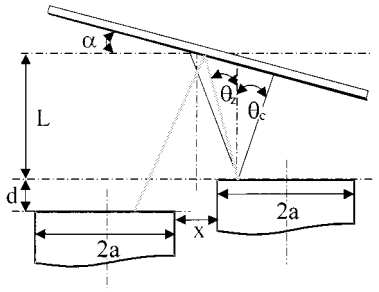

Fig. 3. Parameters that characterize the sensor. L: distance from the fibers to the reflecting surface; d: vertical distance between fibers ends; x: horizontal distance between the fibers; a: radius of the core; α: inclination angle of the reflecting surface; θ_c: maximum acceptance angle; θ_z: angle of incidence.

To a first approach, we assumed the reflectivity of the cylinder's tabs to be 1, although we also varied this parameter from 0 to 1 in our computer simulations, arriving at the same qualitative conclusions. The Fresnel reflection at the two fiber-air interfaces is very approximately equal to that obtained by considering normal incidence. Thus, the fraction of reflected power at both fiber ends is $(n - 1/n + 1)^2 = 0.0389$ [11]. To apply the ray tracing method, we also made use of the radial distance r and the angular position φ that define the departure point of the ray in polar coordinates. In addition, we utilized two more angular parameters to determine the ray's direction (Fig. 4), namely, the angle θ_z between the ray and the symmetry axis of the fiber and the angle φ_β, which specifies the azimuthal position of the reflection point. As shown in the figure, θ_z is always smaller than the complementary critical angle θ_c, because this is the condition for rays to be able to propagate in the fiber [12].

For the simulation, we considered about 100 000 rays distributed in different manners. In particular, we simulated a uniform distribution, a random one, and a Lambertian-Gaussian one, and we obtained the same results for the coupling efficiency in all three cases [6]. In addition, POF coupling effects are very important. Our POF's length is 10 m, which is almost sufficient for the modal equilibrium to be reached [12]. The simulation variables were the distance L to the reflecting surface, the radius a of the POF, and the numerical aperture NA. The reflecting surface was assumed to be planar and parallel to the fiber ends.

B. Purely Mathematical Method

We can also obtain the coupling efficiency by means of a different approach, as shown in Fig. 5. Since the reflecting surface

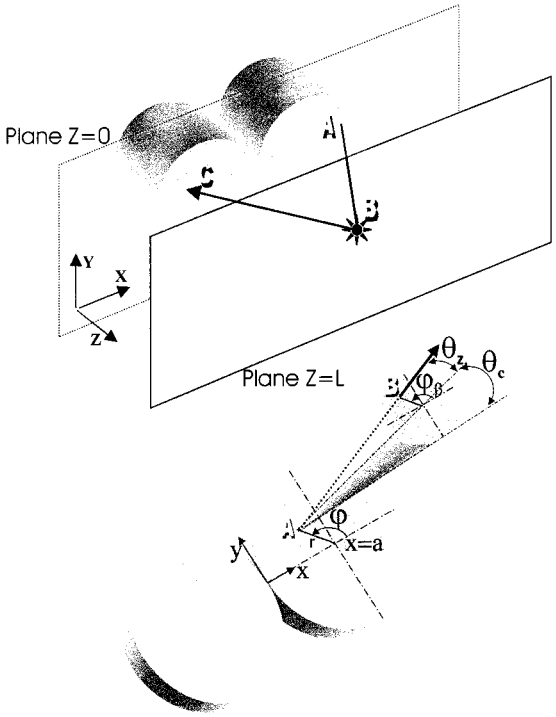

Fig. 4. Parameters that characterize the ray paths.

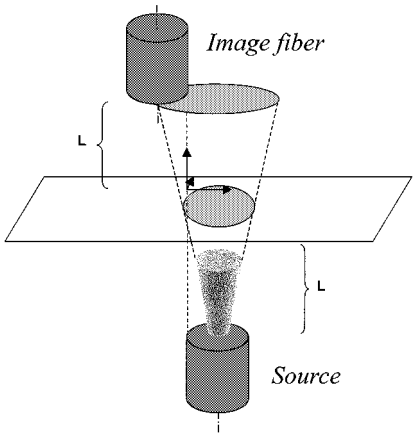

Fig. 5. Geometry of the theoretical model.

behaves as a mirror, those rays initially propagating toward the mirror image of the reception fiber's end will be reflected in a direction that leads to the real fiber's end [13]. As a consequence, the area where this mirror image and the base of the emission cone intersect can be easily related to the coupling efficiency. Specifically, the quotient between this area and the total area of the base of the emission cone is equal to η, provided that the mirror is large enough to reflect all the necessary rays. Otherwise, we would have to consider a smaller emission cone and the response would depend on the exact position of the mirror at a given instant, as we will explain when we analyze the transient response. The procedure is explained *in extenso* in Appendix I.

By calculating the intersection area, we find two solutions for the coupling efficiency as a function of the adimensional parameter χ, shown in (1) at the bottom of the page, where χ is given by $\chi = (L \tan \theta_{\max}/2a)$.

IV. Variation of the Coupling Efficiency With Time

As the angle of aperture of the emitted light cone is θ_c and the distance from the base to the vertex is $2L$, the radius of the base is equal to the radius a of the emission fiber plus the amount $2L \tan \theta_c$. Therefore, the reception fiber will be completely illuminated when $2L \tan \theta_c \geq 2a$, assuming that the horizontal distance x between the two fibers is zero and that all the rays that are directed toward the mirror image of the reception fiber will reflect on the mirror. However, this last condition is only fulfilled during a short interval of time because of the movement of the cylinder's tabs. Therefore, there is a transient variation in the fiber's illuminated area when the reflecting tab enters and exits the light cone. In our case, the rays that will reflect toward the reception fiber are contained in a cylinder whose bases are the end of the emission fiber and the end of the image of the reception fiber. As the mirror crosses this imaginary cylinder at a height L, which is halfway between the two bases, a varying portion of the cylinder's horizontal section is covered. This section is a circle of radius a whose center is located on the imaginary vertical line that is tangent to both fibers. This circle should be completely covered by the mirror for the coupling efficiency to be maximum. The instantaneous coupling efficiency begins to have a value different from zero when the mirror just starts to cover the cylinder's circle. While the mirror does not cover the full circle, we need to consider emission cones of narrower aperture angles, which just touch the edge of the mirror. The coupling efficiency is then calculated in a similar way to that used for the maximum value, but now the radius and the center of the base of the emission cone change with time. The result obtained is shown in (2) at the bottom of the page.

Fig. 6 shows the coupling efficiency as a function of the adimensional parameter q, which is directly proportional to time. As we expected, there are nonzero transition times between the cases of maximum and minimum coupling efficiencies. The transitions have been plotted in a larger scale than the rest of the figure for a better visualization. We can see that longer response times are obtained for greater values of χ or, equivalently, for longer distances between the fibers and the reflecting surface and for smaller diameters.

V. Influence of the Sensor's Structure on the Maximum Coupling Efficiency

The results we present in Figs. 7–9 correspond to the model used to implement our prototype, i.e., $d = x = \alpha = 0$ (the

$$\eta = \left\{ \begin{array}{ll} \frac{1}{4(0.5+\chi)^2} & \text{if } \chi \geq 1 \\ \frac{\pi(1+2\chi+2\chi^2) - \sin^{-1}(1-\chi(\chi+1)) - (1+2\chi)^2 \sin^{-1}\left[\frac{1+\chi(\chi+1)}{1+2\chi}\right] - 2\sqrt{\chi(2+\chi-2\chi^2-\chi^3)}}{4\pi(0.5+\chi)^2} & \text{if } \chi \leq 1 \end{array} \right\}. \quad (1)$$

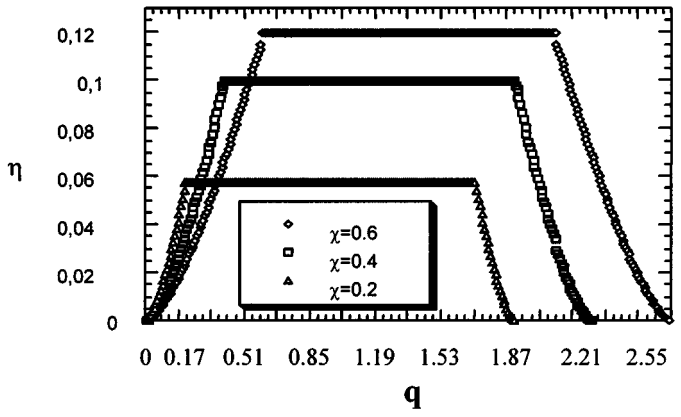

Fig. 6. Variation of the coupling efficiency with time. PMMA POF, $\mathrm{NA} = 0.467, d = x = \alpha = 0; \theta_c = 0.486$ rad (purely mathematical method).

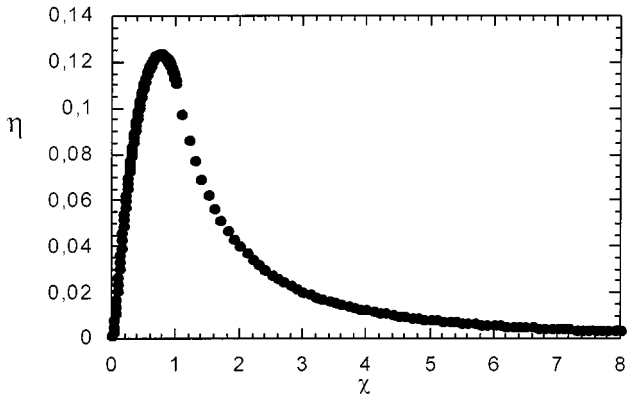

Fig. 7. Coupling efficiency against χ; PMMA POF, $\mathrm{NA} = 0.467, d = x = \alpha = 0; \theta_c = 0.486$ rad (purely mathematical method).

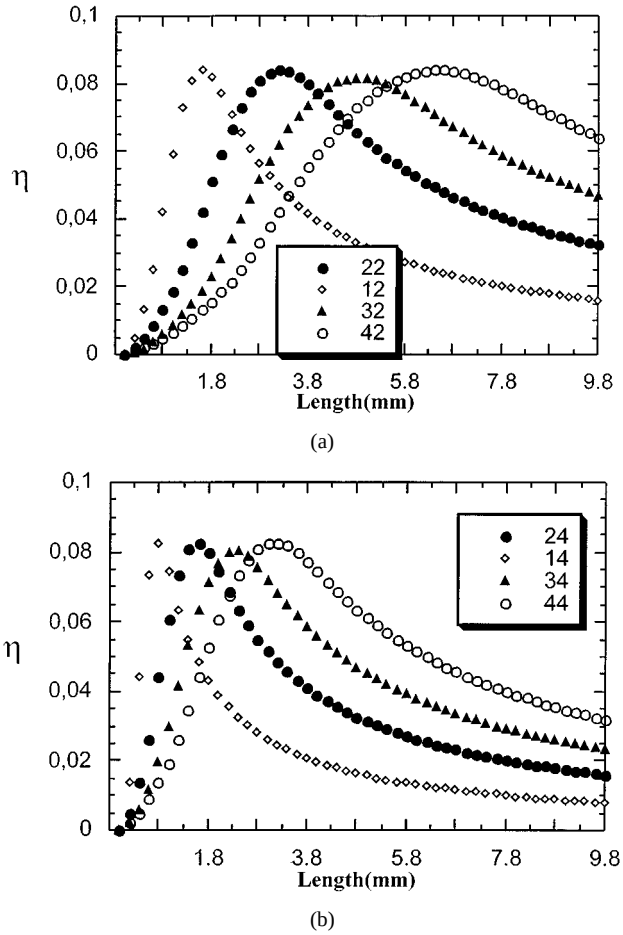

Fig. 8. Coupling efficiency as a function of the fiber radius. The first digit indicates the values of the fiber diameter: 1 = 0.25 mm, 2 = 0.5 mm, 3 = 0.75 mm and 4 = 1 mm. The second digit stands for the NA: 2 = 0.2, and 4 = 0.4 (ray tracing method).

two fibers are touching each other, with no vertical displacement between the fiber ends).

In Fig. 7, we have plotted η versus χ. With the mathematical model, we have obtained the same results as with the ray tracing method, assuming a uniform power distribution. We can observe that there is an optimum value of χ for which the power coupled into the receiving fiber is maximum ($\chi \approx 0.76$). The expressions for the coupling efficiency can also be applied to the study of the influence of the fiber diameter and the numerical aperture (NA). These results are shown in Figs. 8 and 9 for a slightly nonuniform power distribution.

For a fixed NA, an increase in the fiber radius shifts the maximum value toward longer distances, this effect being more significant for small numerical apertures. This phenomenon is depicted in Fig. 8 for $\mathrm{NA} = 0.2$ 8(a) and $\mathrm{NA} = 0.4$ 8(b) and diameters ranging between 0.25 mm and 1 mm. We can observe that the results are very similar for $2a = 0.25$ mm with $\mathrm{NA} = 0.1$ and for $2a = 0.5$ mm with $\mathrm{NA} = 0.2$. The same happens for $2a = 0.5$ mm with $\mathrm{NA} = 0.1$ and for $2a = 1$ mm with $\mathrm{NA} = 0.2$. Such behavior is based on the scale transformation implicit in the parameter χ. If the NA remains unchanged, the coupling efficiency becomes flatter in the proximity of the maximum as the fiber diameter increases.

To discuss the effect of the NA it is more convenient to express χ as $\chi = (\mathrm{LNA}/2a\sqrt{1-\mathrm{NA}^2})$. Fig. 9 shows the results for $2a = 250\ \mu$m 9(a) and $2a = 500\ \mu$m 9(b), with numerical apertures in the range between 0.1 to 0.5. As the NA grows, the maximum value of the curve moves toward smaller distances. We can see that the peaks of η occur for shorter values of L in the case of small diameters and high numerical apertures. For small values of the NA, the maximum of the curve spreads out, which facilitates the sensor's mechanical design because the influence of L becomes less important. For high values of the NA,

$$\eta(t) = \frac{(\chi+q+1)^2[v_i+\pi/2+0.5\sin 2v_i]+[\pi/2-\omega_i-0.5\sin 2\omega_i]}{4\pi(0.5+\chi)^2}$$

$$\text{where } q = vt/2a; \quad \sin v_i = -\frac{q^2+(1+q)^2+(1+\chi-q)}{(1+\chi+q)(2+\chi-q)}; \quad \sin\omega_i = 1-\frac{2q(1+\chi)}{(2+\chi-q)}. \tag{2}$$

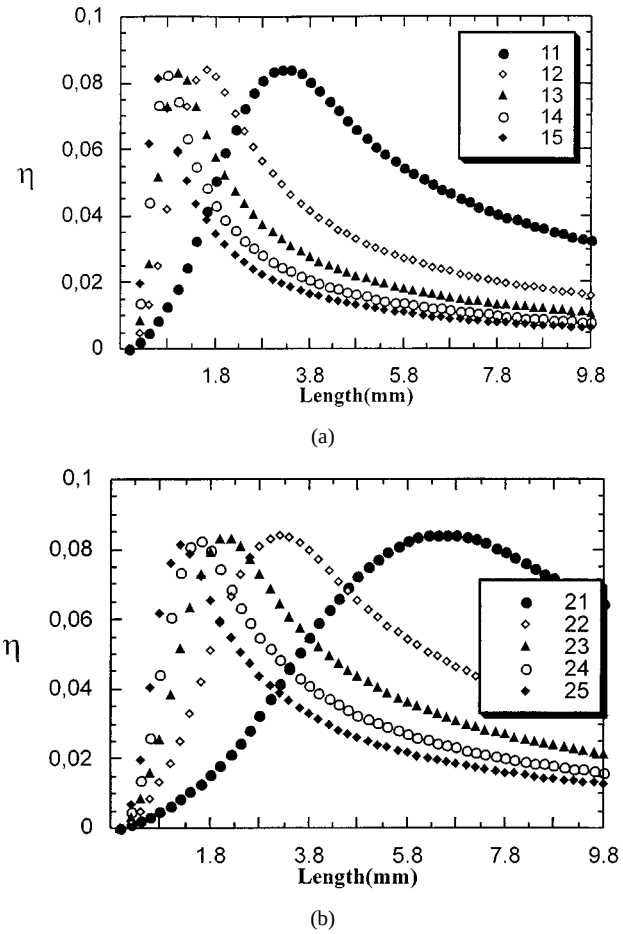

(a)

(b)

Fig. 9. Coupling efficiency as a function of the NA. The first digit stands for the fiber diameter: 1 = 0.25 mm and 2 = 0.5 mm. The second digit indicates the values of the NA: 1 = 0.1, 2 = 0.2, 3 = 0.3, 4 = 0.4, and 5 = 0.5 (ray tracing method).

the deviations from the optimum L are very critical, which increases the probability of error in the mechanical design. As the core radius increases, the distance for which the coupled power is maximum increases as well. In all cases, the coupling efficiency η is around 8%.

In Fig. 6, we present the simulated results of the sensor's response corresponding to several fiber diameters and to a wind speed of 1 turn per second at the anemometer. We can see that the response time is longer for small-diameter fibers. Therefore, fibers of larger diameters yield a better transient response. Generalizing the result, shorter response times are obtained for smaller values of χ or, equivalently, for shorter distances between the fibers and the reflecting surface or for larger diameters.

VI. Experimental Results

Fig. 10 shows the experimental results as a function of the distance L between the fibers and the reflecting surface for two different fiber diameters. The received powers were normalized to the unity in both cases for the sake of comparison. Their behavior coincides with that of the simulations, although the separation between the two maximums is greater than that predicted in the simulations. The reason for this seems to be the small separation x between the fibers in practice, which was not taken into account in our simulations (in Fig. 3, we took $x = 0$).

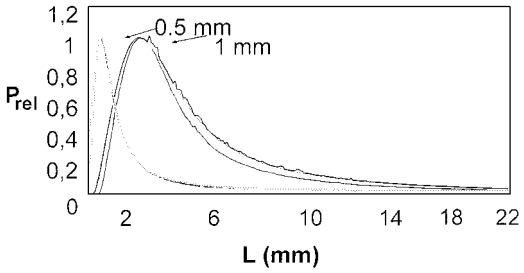

Fig. 10. Experimental results of the sensor's response for different fiber diameters. $P_{\rm rel}$ means normalized received optical power.

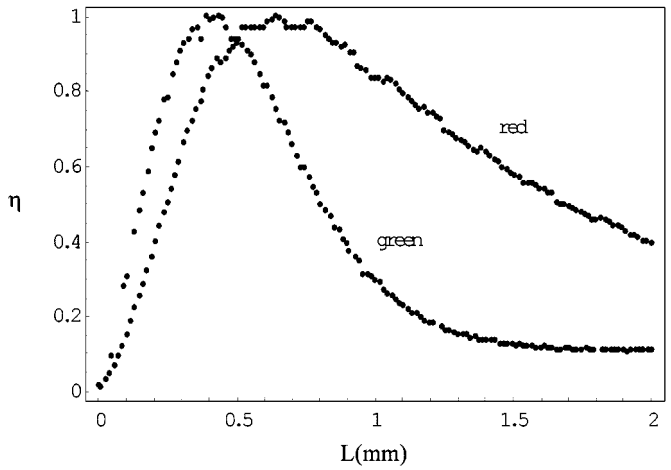

Fig. 11. Coupling efficiency as a function of wavelength. PMMA POF, $2a$ = 0.49 mm, NA = 0.467.

Fig. 11 shows the coupling efficiency as a function of the distance from the fibers to the mirror for two different wavelengths (He–Ne at 632.8 and at 543 nm) when keeping the rest of the parameters fixed. These wavelengths were chosen for their easy availability in the market and wide use in industry (green and red LEDs) and also because they correspond to the minimum of attenuation of PMMA. It can be seen that for green light, the response is more abrupt, which implies less manufacturing tolerance. Another inconvenience is that the maximum efficiency occurs at smaller distances. For that reason, we chose a red LED in our final design.

We can also note that Fig. 11 displays the same features as Fig. 9. From the observation of both figures we find that the behavior observed for green light can be due to an increase in the POFs numerical aperture for that wavelength, i.e., the POFs numerical aperture depends on the wavelength. The maximum coupling efficiency is located at $L = 0.4$ mm for the green He–Ne laser and at $L = 0.6$ mm for the red one. This implies that the numerical aperture for 543 nm should be 1.27 times greater than that for 632.8 nm (in both cases we have assumed that the maximum occurs when $\chi = 0.76$, as it turns out from the simulations and from the mathematical method). On the other hand, the refractive index of PMMA varies from 1.5 at 450 nm to 1.49 at 700 nm, although this variation cannot explain the observed behavior. In addition, we do not know the dispersion of the cladding material. The discrepancy could also be

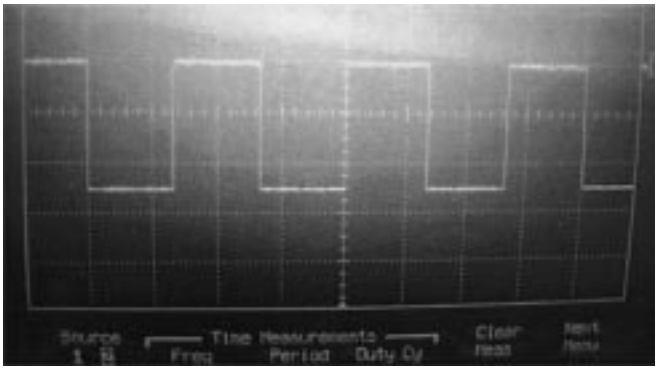

Fig. 12. Experimental square wave obtained in the oscilloscope. PMMA, $\mathrm{NA} = 0.467$, $\lambda = 660$ nm, $2a = 0.5$ mm, $L = 1.2$ mm, $v = 15$ km/h, and $V_{\mathrm{pp}} = 20$ V. The time corresponding to the complete horizontal axis is 0.12 s.

TABLE I
TECHNICAL DATA OF THE SPEED SENSOR

Temperature range	-25°C –70°C
Core diameter	0.49 mm
Number of fibres (emission/reception)	1/1
Transmitter/receiver	Contrinex LFK-3031-303 Voltage=10-36 V ; I=200 mA Output V_{pp}< 20 V
Fiber length	10 m
Wind speed range	10-60 Km/h
POF	Step-index PMMA NA=0.467
Typical coupling efficiency	5 %
Distance fibers-mirror	0.4 mm
Wavelength (LED)	660 nm

caused by the increase in the number of modes for shorter wavelengths, which, in connection with the parameter V, is equivalent to increasing the numerical aperture while maintaining the same wavelength. In addition, a small variation of the input light conditions at the entrance of the POF, such as a small tilt of the lasers, could be partially responsible of the difference observed for the two lasers. For example, a difference of 6° in the output light could explain the results. Anyway, we believe that all of these factors together contribute to explain the results.

To improve the performance of the device we used a variation of our original design. In the new device we used one emission POF and six reception fibers. The structure consisted of an emitting fiber located in the middle of the hexagon formed by the six reception fibers (one at each vertex of the hexagon). The experimental results, which are not shown here for the sake of abbreviation, display a broadening in the efficiency curve at longer lengths and a small shift of the maximum. In any case, the results are too similar to those corresponding to a single pair of fibers for the use of seven fibers, instead of two, to be worth.

Fig. 12 shows the experimental square wave received for a wind speed of 15 km/h using a 0.5 mm core diameter PMMA POF located at a distance $L = 1.2$ mm (to the right of the maximum) from the reflective tabs. As we can see, it is very simple to distinguish between the periods of time during which a slot is passing in front of the fibers and those during which a cylinder's tab is passing. The output voltage was 20 V, which is an easy value to measure. Table I serves as a summary of the main characteristics of our device. It is seen that the sensor can work at any temperature in the range between -25 and $+70^{\circ}$ C. Wind speeds greater than 60 km/h do not need to be measured, because the wind generator's vanes stop at such speeds for safety reasons. However, our sensor can work at much higher speeds (100 km/h). The required fiber length was 10 m, as this was the real distance between the sensor and the generator's automaton. The coupling efficiency is generally low (∼5%), just a bit smaller than the predicted one (∼8%), because the reflecting surface is not an ideal mirror as it was assumed. This could be improved by using polished reflecting surfaces. Anyway, a low coupling efficiency can be compensated if necessary by means of high sensitivity receptors.

VII. CONCLUSION

We have developed an optical POF-based sensor to determine the wind speed in wind generators. We have found that a tradeoff between a large fiber diameter (which relaxes the mechanical design's tolerances) and a small one (which reduces bending losses in the box containing the anemometer) is required to optimize the sensor's response. Our sensor is immune to the electromagnetic interference provoked in storms and it has a long lifetime. It can work in a wide range of temperatures, and it can be used to measure wind speed in the range between 10 and 100 km.

APPENDIX I

In this section, we will derive the expression for the coupling efficiency η. As a function of χ we can distinguish between two cases for the calculus of the coupling efficiency, namely, $\chi < 1$ and $\chi > 1$.

A. $\chi > 1$

In this case $2L\tan\theta_{\max} > d$, where L is the distance from the fiber to the mirror, d is the fiber core diameter, and $\theta_{\max}$ is the maximum angle of acceptance. The power reflected back to the fiber can be calculated from the ratio of the light emitting cone area $A_{\mathrm{emittingcone}}$ and the fiber core area $A_{\mathrm{fibercore}}$, i.e.,

$$\eta = \frac{P_{\mathrm{received}}}{P_{\mathrm{emitted}}} = \frac{A_{\mathrm{fibercore}}}{A_{\mathrm{emittingcone}}} = \frac{\pi d^2/2}{\pi(d/2 + 2l\tan\vartheta_{\max})^2} = \frac{\pi d^2/2}{\pi(d/2)^2(1+2\chi)^2} = \frac{1}{(1+2\chi)^2} \tag{I.1}$$

where we have considered that the emitted power is uniformly distributed.

B. $\chi < 1$

In this situation, only part of the fiber core is illuminated by the reflected light. Fig. 13 represents this case. Therefore, the coupling efficiency will be the intersection area of the light-emitting cone, and the fiber core divided by the light emitting

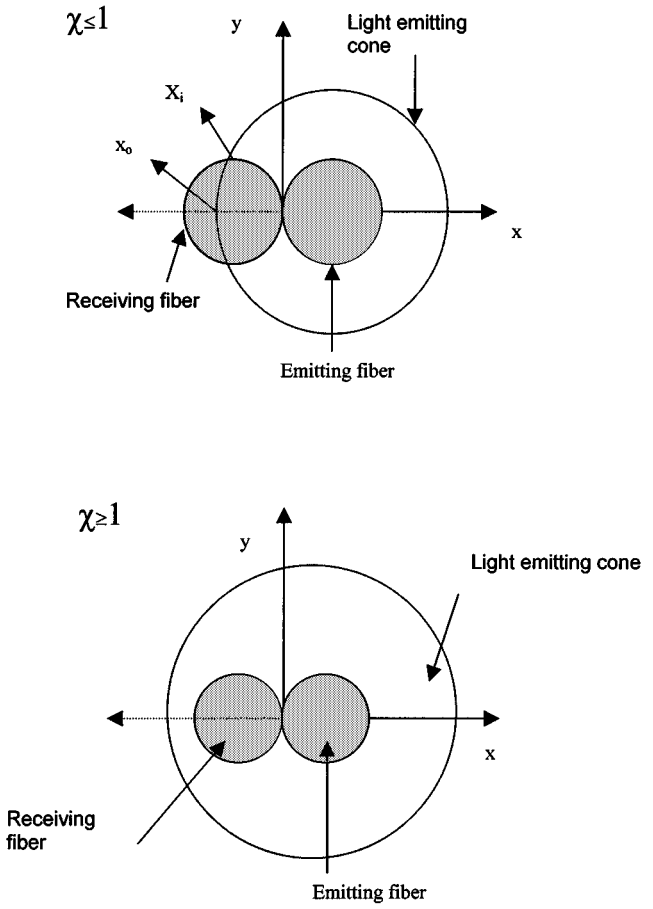

Fig. 13. Relationship between the light emitting cone's radius and the receiving fiber's radius for the cases $\chi \geq 1$ and $\chi \leq 1$. $\mathbf{x_i}$ and $\mathbf{x_o}$ stand for the coordinate of the intersection between the light emitting cone and the x axis and that between the light-emitting cone and the receiving fiber, respectively.

cone area (of radius R). From the equations of these two circumferences

$$d^2/4 = y^2 + (x + d/2)^2$$
$$R^2 = y^2 + (x - d/2)^2 \tag{I.2}$$

we can deduce the points x_o and x_i. The intersection area will be

$$\begin{aligned} A_{\text{intersection}} &= 2\int_{x_0}^{x_i} \sqrt{R^2 - (x - d/2)^2} \\ &\quad + 2\int_{x_0}^{x_i} \sqrt{d^2/4 - (x + d/2)^2} \\ &= (d/2)^2\pi(1 + 2\chi + 2\chi^2) \\ &\quad - \sin^{-1}(1 - \chi(\chi + 1)) \\ &\quad - (1 + 2\chi)^2 \sin^{-1}\left[\frac{1 + \chi(\chi + 1)}{1 + 2\chi}\right] \\ &\quad - 2\sqrt{\chi(2 + \chi - 2\chi^2 - \chi^3)}. \end{aligned} \tag{I.3}$$

As before, the coupling efficiency will be calculated from the ratio of this area to that of the emitting cone

$$A_{\text{emittingcone}} = \pi(d/2)^2(1 + 2\chi)^2. \tag{I.4}$$

This ratio leads immediately to expression 1. Following the same procedure, (2) is easily obtained by taking into account that in this case, the radius of the light emitting cone depends on time $R = d\,(1 + 2q)$, where $q = vt/d$, and v is the speed of the rotating reflecting surface.

REFERENCES

[1] B. D. Gupta and S. K. Khijwania, "Experimental studies on the response of the fiber optic evanescent field absorption sensor," *Fiber Integrated Opt.*, vol. 17, pp. 63–73, 1998.
[2] C. Davis, *Fiberoptic Sensor Technology Handbook*. Herndon, VA: Optical Technol., 1986.
[3] B. Culshaw and J. Dakin, *Optical Fiber Sensors*. Norwood, MA: Artech House, 1995–1997.
[4] D. A. Krohn, *Fiber Optic Sensors*: Instrument Soc. Amer., 1992.
[5] Y. Koike, "Progress in GI-POF status of high speed plastic optical fiber and its future prospect," in *Proc. POF Conf.*, 2000, pp. 1–5.
[6] J. Zubia, G. Garitaonaindía, and J. Arrue, "Passive device based on plastic optical fibers to determine the indices of refraction of liquids," *Appl. Opt.*, vol. 39, no. 6, pp. 941–946, 2000.
[7] J. Arrue, J. Zubia, G. Fuster, and D. Kalymnios, "Light power behavior when bending plastic optical fibers," *IEE Proc. Optoelectron.*, vol. 145, Dec. 1998.
[8] D. Gloge, "Optical power flow in multimode fibers," *Bell Syst. Tech. J.*, vol. 51, pp. 1767–1783, 1972.
[9] A. W. Snyder and D. J. Mitchell, "Generalized fresnel's laws for determining radiation loss from optical waveguides, and curved dielectric structures," *OPTIK*, vol. 40, no. 4, pp. 438–459, 1974.
[10] A. W. Snyder and J. Love, *Optical Waveguide Theory*. London, U.K.: Chapman and Hall, 1983.
[11] M. Born and E. Wolf, *Principles of Optics*. Oxford, U.K.: Pergamon, 1986.
[12] G. Jiang, R. F. Shi, and A. F. Garito, "Mode coupling and equilibrium mode distribution condition in plastic optical fibers," *IEEE Photon Technol. Lett.*, vol. 9, no. 8, pp. 1128–1130, 1997.
[13] G. Economou and D. E. N. Davies, "Studies of optical fiber displacement sensor," *J. IEEE*, vol. 57, no. 2, pp. 63–66, 1987.
[14] T. Ishigure, E. Nihei, and Y. Koike, "Optimum refractive index profile of the graded-index polymer optical fiber, toward gigabit data links," *Appl. Opt.*, vol. 35, no. 12, pp. 2048–2053, 1996.

Joseba Zubia received the degree in solid state physics and the Ph.D. degree in physics from the Faculty of Science, University of the Basque Country, Bilbao, Spain, in 1988 and 1993, respectively, focusing on optical properties of ferroelectric liquid crystals.

He is an Associate Professor with the Telecommunications Engineering School, University of the Basque Country. With over six years of experience doing basic research in the field of plastic optical fibers, he has accumulated a wealth of knowledge in this field. At present, he is involved in research projects in collaboration with universities and companies from Spain and other countries in the fields of plastic optical fibers, fiber optical sensors, and liquid crystals.

Dr. Zubia won the special award for Best Thesis in 1995.

O. Aresti, photograph and biography not available at the time of publication.

Jon Arrúe received the degree in electronic physics from the University of the Basque Country, Bilbao, Spain, and the M.S. degree in electronics and in telecommunications and the European Ph.D. in the field of optical fibers from the Telecommunications Engineering School, University of the Basque Country, in 1999, both of which were awarded with the maximum marks.

He is a Lecturer with the Telecommunications Engineering School, University of the Basque Country. He has been involved in international research projects since several years ago.

M. López-Amo, photograph and biography not available at the time of publication.